Contents list available at CBIORE journal website

International Journal of Renewable Energy Development

Journal homepage: https://ijred.cbiore.id

Research Article

Enhancing hierarchical factor (HF) and catalytic performance of Bayah's natural zeolite catalyst for hydrocracking of palm oil to biofuels

I. Istadi [a,b*], Wais Alqurni [a,b], Teguh Riyanto [b,c]

[a]*Department of Chemical Engineering, Faculty of Engineering, Universitas Diponegoro, Semarang, Central Java, 50275, Indonesia.*

[b]*Laboratory of Plasma-Catalysis (R3.5), Center of Research and Service – Diponegoro University (CORES-DU), Integrated Laboratory, Universitas Diponegoro, Semarang, Central Java, 50275, Indonesia.*

[c]*Industrial Chemical Engineering Technology, Vocational College, Universitas Diponegoro, Semarang, Central Java, 50275, Indonesia.*

Abstract. This study investigates enhancement of Bayah's Natural Zeolite (BNZ), an abundant resource from Banten, Indonesia, as a catalyst for hydrocracking palm oil into biofuels. The primary objective was to improve the zeolite's Hierarchical Factor (HF) and overall catalytic performance through a targeted modification process. The modification involved a two-step procedure: a desilication treatment using various concentrations of sodium hydroxide (NaOH) to create mesoporosity, followed by activation with an ammonium acetate (CH_3COONH_4) solution. The structural, textural, and chemical properties of the modified catalysts were systematically characterized using X-ray Diffraction (XRD), X-ray Fluorescence (XRF), and Brunauer-Emmett-Teller/Barrett-Joyner-Halenda (BET-BJH) analysis. The characterization results revealed that the NaOH treatment increased the HF, average pore diameter, pore volume, and specific surface area compared to the untreated BNZ. Catalytic performance was evaluated in a continuous hydrocracking reactor using palm oil as feedstock. Among the modified samples, the BNZ-3 catalyst exhibited the most promising activity, demonstrating an optimal average pore diameter of 3.83 nm and an HF value of 0.069. This catalyst achieved an impressive Organic Liquid Product (OLP) yield of 85.67% and a palm oil conversion rate of 97.22%. The conversion of triglycerides was monitored via Fourier Transform Infrared Spectroscopy (FT-IR) by observing the disappearance of the ester bond absorption peak at 1745 cm^{-1}. Furthermore, Gas Chromatography-Mass Spectrometry (GC-MS) analysis of the distilled biofuel confirmed the presence of desired hydrocarbons fractions, including gasoline, kerosene, and diesel components, alongside minor quantities of alcohols, esters, and acids. The DSC results corroborate the TG and DTG analyses, reinforcing the conclusion that BNZ-3 experiences more extensive coke deposition and undergoes more intense thermal decomposition than the blank catalyst. These findings underscore the potential of modified natural zeolites as effective, low-cost catalysts for sustainable biofuel production.

Keywords: Hydrocracking; Palm Oil; Biofuel; Bayah's Natural Zeolit (BNZ); Hierarchical Factor (HF).

@ The author(s). Published by CBIORE. This is an open access article under the CC BY-SA license (http://creativecommons.org/licenses/by-sa/4.0/).

Received: 13th August 2025; Revised: 18th Nov 2025; Accepted: 16th Dec 2025; Available online: 3rd January 2026

1. Introduction

Energy consumption has risen over the years due to the increasing energy demands of a growing global population (Mortensen *et al.*, 2011). Primary sectors contributing to this increase encompass transportation, heating systems, electricity generation, and energy use within the residential and industrial sectors. Among these, the transportation sector is particularly notable, accounting for about 20% of global energy demand. The reliance on fossil fuels, which are non-renewable and subject to price volatility, is becoming increasingly unsustainable. Additionally, fossil fuel exploration has likely reached its peak, highlighting the urgent need for alternative, sustainable energy sources that are environmentally friendly and do not emit greenhouse gases (Mortensen *et al.*, 2011; Alaba *et al.*, 2016). One promising renewable energy source is vegetable oil, primarily composed of triglycerides. These triglycerides, found in both animal fats and plant oils, are already being used as feedstock for biofuel production (Nasikin *et al.*, 2009; Long *et al.*, 2020).

Vegetable oils are commonly used as feedstock in the production of biofuels, with examples including palm oil (Panarmasar *et al.*, 2022; Istadi *et al.*, 2020; Dewanti *et al.*, 2022; Istadi *et al.*, 2024), jatropha oil (Aziz *et al.*, 2021), soybean oil (Zheng *et al.*, 2019), and sunflower oil (Seifi *et al.*, 2016). Among these, palm oil stands out as the most promising alternative due to its high yield, especially in tropical regions such as Indonesia, which produced approximately 47.474 million tons in 2024 (Nasikin *et al.*, 2009; Badan Pusat Statistik 2025). Analysis of refined palm oil from local markets shows that it contains 43.30% palmitic acid (a saturated fatty acid) and 18.51% oleic acid (an unsaturated fatty acid). The remaining 38.19% consists of various other compounds, including 1-nonadecene, 11-hexacosyne, oleic acid-3-(octadecyloxy) propyl ester, 9-tricosene, (Z,Z)-3,9-cis-6,7-epoxy-nonadecadiene, Z-13-

* Corresponding author
Email: istadi@che.undip.ac.id (I. Istadi)

https://doi.org/10.61435/ijred.2026.61669
ISSN: 2252-4940/© 2026.The Author(s). Published by CBIORE

octadecenyl acetate, 2-pentadecanone, 1-heptadecanol, and 2-monopalmitin (Istadi *et al*., 2020). Palm oil can be converted into biofuels through various cracking techniques, such as thermal cracking, catalytic cracking, and catalytic hydrocracking. Among these, the catalytic hydrocracking is particularly effective, offering high conversion rates and reduced oxygen content in the final product. This is largely due to the role of hydrogen in minimizing oxygen levels during the process (Istadi *et al*., 2021). The cracking of palm oil can yield several types of biofuels, including biogasoline (Istadi *et al*., 2020; Dewanti *et al*., 2022; Istadi *et al*., 2021; Kadarwati *et al*., 2015), kerosene (Istadi *et al*., 2020; Aziz *et al*., 2021), bioavtur (Panarmasar *et al*., 2022; Dewanti *et al*., 2022), and green diesel (Istadi *et al*., 2020; Dewanti *et al*., 2022). The efficiency of catalytic hydrocracking depends heavily on the characteristics of the catalyst used, such as pore diameter, pore volume, structure, and surface area (Panarmasar *et al*., 2022).

One example of a catalyst used in this process is Bayah's Natural Zeolite (BNZ), which is notable for its natural abundance in Indonesia and cost-effectiveness. However, due to its high impurity content, the BNZ must undergo preparation and modification before it can be effectively used in the cracking process. To enhance its catalytic performance, the BNZ catalyst must undergo activation and modification. A common limitation of both natural and synthetic zeolites is their microporous structure, which can hinder the movement of larger molecules (Abelló *et al*., 2009; Oliveira *et al*., 2023). In the case of large reactants like palm oil, this can lead to diffusion resistance when molecules attempt to access or exit the active sites. To address this issue, natural zeolites need to be transformed into a hierarchical structure with mesoporous characteristics. This transformation can be achieved through a process called desilication, which modifies the zeolite to allow better diffusion of larger molecules (Aziz *et al*., 2021).

Desilication is a technique used to remove silica from the zeolite framework by treating it with an alkaline solution, which reduces the silica content in the natural zeolite structure (Abelló *et al*., 2009; Groen *et al*., 2006). This process enhances the formation of mesopores and significantly increases the surface area of the catalyst, leading to improved reactivity and efficiency (Aziz *et al*., 2021; Abelló *et al*., 2009; Groen *et al*., 2005). Both synthetic and natural zeolites have been successfully modified through desilication, resulting in enhanced catalytic performance. Examples of zeolites that have shown positive results after desilication include ZSM-5 (Abelló *et al*., 2009; Li *et al*., 2020), ZSM-12 (Akyalcin *et al*., 2019), ZSM-48 (Azhari *et al*., 2023), BEA (Groen *et al*., 2008; Verboekend *et al*., 2012), Zeolite T (Yin *et al*., 2015), USY (Verboekend *et al*., 2012), Zeolite Y (Garcia *et al*., 2015; Oruji *et al*., 2018), MCM-22 (Mokrzycki *et al*., 2009), Mordenite (Groen *et al*., 2007), and Klinoptilolite (Akgül *et al*., 2011; Aziz *et al*., 2023). In total, around 24 different types of zeolites have been effectively treated using this method (Oliveira *et al*., 2023).

The catalytic activity of hierarchical mesoporous zeolite in the BNZ depends on the hierarchical factor (HF). Several HF values presented in (Table 1) are compared with those from this study, indicating that the highest HF value obtained is closely aligned with the comparison. The hierarchical factor is a precise tool for categorizing the degree of the structure of porous materials. The zeolite catalysts with higher HF often show high catalytic performance compared to catalysts synthesized from the same precursor (Chen *et al*., 2020). Eq. (1) is the expression for obtaining HF:

$$HF = \frac{V_{\text{micro}} \times S_{\text{meso}}}{V_{\text{total}} \times S_{BET}} \quad (1)$$

where V_{micro} is the micropore volume, V_{total} is the total pore volume, S_{meso} is the mesopore surface area, and S_{BET} is the BET surface area (Chen *et al*., 2020). This research presents a novel investigation into the significant enhancement of the Hierarchical Factor (HF) of Bayah's natural zeolite, an abundant resource in Banten, Indonesia, which has not been explored in previous studies. The modified Bayah's Natural Zeolite (BNZ) catalyst demonstrates promising potential for application in catalytic hydrocracking of palm oil into biofuels. To improve its catalytic properties, the BNZ was subjected to desilication using sodium hydroxide (NaOH) as the alkaline agent, followed by activation with ammonium acetate under varying conditions. These treatments aimed to increase the HF, pore diameter, pore volume, and surface area of the zeolite. The study specifically examines how variations in NaOH concentration, treatment temperature, and desilication duration influence the structural characteristics of the catalyst, with a focus on HF. While the desilication process enhances the HF and catalytic performance, it also leads to a reduced Si/Al ratio due to silica removal. Overall, increasing the HF of Bayah's Natural Zeolite significantly improves its efficiency in the deoxygenation of palm oil, thereby advancing its suitability for biofuel production.

2. Materials and Method

2.1 Materials

This study utilized Bayah's Natural Zeolite (BNZ) as the catalyst material, which was supplied by PT Minerindo Trifa Buana. For the desilication and activation processes, sodium hydroxide (NaOH, 99.5% purity, Merck) and ammonium acetate

Table 1
Comparison of Reported Hierarchical Factor (HF)

No	Catalyst	Reported Maximum HF Value	Treatment Method	Catalyst Origin	Ref
1	Hierarchical ZSM-5	0.09	Surfactant-assisted hydrothermal synthesis	Synthetic	Karim, T. M., et al. (2024).
2	Cu/ZSM-5	0.115	Protective alkali-etching with TPA^+	Synthetic	Guo, X., et al. (2024).
3	H/Zn-ZSM-5	0.14	Zn modification and hierarchical structuring	Synthetic	Mamman, J. T., et al. (2022)
4	ZSM-5 (MFI)	0.26	Hydrothermal synthesis	Synthetic	Parkhomchuk, E. V., et al. (2019).
5	Hierarchical Bayah Natural Zeolite	0.069	Desilication NaOH	Natural	This Study

(CH_3COONH_4, 99.6% purity, Merck) were used, respectively. The feedstock consisted of refined palm oil purchased locally under the brand Tropical. Hydrogen gas with 99.99% UHP purity was employed during the catalytic hydrocracking process. Additionally, nitrogen gas (99% UHP) was used in the flashing process to purge oxygen from the piping and reactor system.

2.2 Preparation of the BNZ catalysts

To prepare the catalyst, large chunks of Bayah's Natural Zeolite (BNZ) were first crushed and ground to a fine powder with a mesh size of 16. The sieved material was then dried in a Memmert electric oven at 105 °C for one hour. Desilication was carried out using a sodium hydroxide (NaOH) solution. Specifically, 20 grams of BNZ were placed in a beaker and mixed with 400 mL of NaOH solution under varying conditions. The desilication process employed ultrasonic stirring, with independent variables including NaOH concentration (0.2, 0.4, 0.5, and 0.6 M), stirring temperature (room temperature, 45 °C, and 65 °C), and stirring duration (30, 60, and 120 minutes). The reference conditions, 0.5 M NaOH, 65 °C, and 30 minutes, were selected based on prior research findings (Aziz *et al*., 2024).

After the desilication, the zeolite was rinsed with distilled water and dried. It was then activated by treating it with 200 mL of 1 M ammonium acetate (CH_3COONH_4) at 90 °C for 5 hours using conventional stirring at 300 rpm. The activated zeolite was washed until neutral, dried, and then calcined at 550 °C for 3 hours (Aziz *et al*., 2024). The untreated catalyst was labeled BNZ-NT, while the base-treated samples, modified under different NaOH concentrations, temperatures, and treatment times, were labeled BNZ-1 through BNZ-8 (details provided in Table 2). Finally, the catalysts were pelletized, crushed, and sieved to a particle size of 18 mesh.

2.3 Catalysts Characterizations

Various characterization techniques were employed to analyze the properties of the catalysts. These particle properties included surface area, pore volume, pore diameter, hierarchical factor (HF), elemental composition, and crystal structure. The surface area was measured using the Brunauer–Emmett–Teller (BET) method, while pore volume and pore size were determined using the Barrett–Joyner–Halenda (BJH) method. The external surface area was calculated using the t-plot method. All BET and BJH analyses were conducted through nitrogen gas physisorption using a ChemBET PULSAR Quantachrome instrument. The hierarchical factor was calculated based on surface area and pore volume using Equation (1) (Chen *et al*., 2020). Elemental composition and the Si/Al weight ratio were assessed using X-ray fluorescence (XRF) with a Rigaku Supermini 200 Benchtop WDXRF Spectrometer. To examine the crystal structure, X-ray diffraction (XRD) analysis was performed using a Shimadzu 7000 diffractometer with Cu-Kα radiation (λ = 1.54056 Å), operated at 30 mA and 40 kV. Diffraction patterns were recorded over a 2θ range of 10° to 90° at a scanning rate of 2° per minute.

2.3 Catalyst Performance Testing for Continuous Hydrocracking of Palm Oil to Biofuels

The Bayah's natural zeolite catalysts, which were modified through desilication using NaOH and activated with an ammonium acetate (CH_3COONH_4) solution, were evaluated for their catalytic performance in converting palm oil into biofuel via the catalytic hydrocracking process. Each catalyst, treated based on Table 2, underwent performance testing for continuous hydrocracking of palm oil to biofuels. The setup used a continuous fixed-bed reactor made of stainless steel with a 1-inch diameter (see Figure 1). For each test, 10 grams of the prepared zeolite catalyst were loaded into the reactor, supported by glass wool. To eliminate any residual oxygen in the system, the reactor was purged with 100 mL of nitrogen gas for 15 minutes flowing, ensuring all components and tubing were flushed. An electric heater was used to raise the reactor temperature to 500 °C, with digital controls used to monitor and maintain a stable temperature throughout the process.

The catalyst being tested in a continuous fixed bed catalytic reactor. Refined palm oil and hydrogen gas were introduced into the reactor, with the palm oil fed at a Weight Hourly Space Velocity (WHSV) of 0.365 min^{-1} and hydrogen flowing at a rate of 300 $cm^3.min^{-1}$. The reaction was carried out for 3 hours, beginning after a 30-minute stabilization period to reach steady-state conditions. This was a continuous process, where the resulting products were condensed into an organic liquid product (OLP) and collected in an Erlenmeyer flask, while non-condensable gases were separated. In addition to gas and liquid products, coke was also formed as a by-product of the catalytic cracking process.

The Organic Liquid Product (OLP) obtained from the catalytic hydrocracking process was separated using a distillation apparatus to quantify the amounts of biogasoline, kerosene, and diesel present. This separation relied on the distinct boiling point ranges of each component: 39–204 °C for gasoline, 205–310 °C for kerosene or avtuur, and 310–370 °C

Table 2
Desilication treatment of BNZ zeolite in this study.

Catalyst	NaOH Concentration	Temperature of Desilication	Time of Desilication
	(M)	(°C)	(min)
BNZ-NT*	-	-	-
BNZ-1⁑	0.2	65	30
BNZ-2⁑	0.4	65	30
BNZ-3⁑†‡	0.5	65	30
BNZ-4⁑	0.6	65	30
BNZ-5†	0.5	Room Temperature	30
BNZ-6†	0.5	45	30
BNZ-7‡	0.5	65	60
BNZ-8‡	0.5	65	120

*NT = Non-treatment; ⁑NaOH concentration variation; †Temperature of desilication; ‡Time of desilication; ⁑†‡Catalyst with all variations.

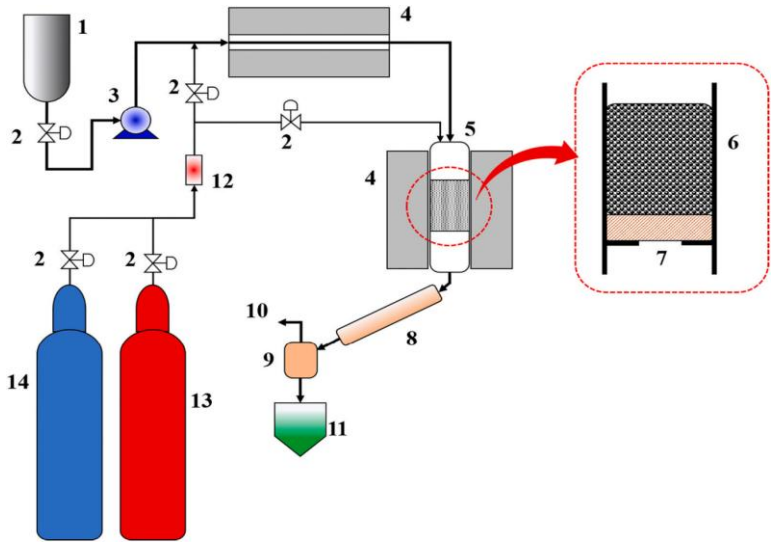

Fig. 1. Scheme of the experimental catalytic hydrocracking set up: (1) Palm oil feedstock tank, (2) Gate valve, (3) Peristaltic pump, (4) Electric heating furnace, (5) Reactor tube, (6) Catalysts packing, (7) Glass wool, (8) Condensor, (9) Gas-liquid separator, (10) Gas by product, (11) Liquid fuels product, (12) Gas flowmeter, (13) Hydrogen gas tank and (14) Nitrogen gas tank.

for diesel (Istadi *et al.*, 2023). The resulting liquid biofuels fractions (gasoline, kerosene, and diesel) were then analyzed using gas chromatography–mass spectrometry (GC–MS) with a QP2010S SHIMADZU system and a DB-1 column to determine their chemical composition. The GC–MS analysis was conducted with an initial oven temperature of 50 °C (held for 5 minutes), followed by a temperature ramp of 10 °C per minute up to 260 °C, where it was maintained for 73 minutes.

To identify the functional groups, present in the liquid products, Fourier-transform Infrared (FTIR) spectroscopy was used. The FTIR spectra were recorded over a wavenumber range of 400–4000 cm^{-1} using a Perkin-Elmer UATR Spectrum Two instrument. The conversion of palm oil (triglycerides) into biofuel was determined by analyzing the absorption area of the carbonyl group at 1745 cm^{-1}. This calculation was performed using Equation (2), where A_{1745} palm oil represents the absorption area at 1745 cm^{-1} for the original palm oil, and A_{1745} biofuel represents the corresponding area for the biofuel product (Istadi *et al.*, 2023).

$$\text{Conversion } (\%) = \frac{A_{1745\ palm\ oil} - A_{1745\ biofuel}}{A_{1745\ palm\ oil}} \times 100\% \qquad (2)$$

The yield and selectivity of the biofuels product obtained from the catalytic hydrocracking process, following distillation, are determined using the equations provided below, where m_i expresses mass of component *i* (gram):

$$\text{Yield of OLP } (\%) = \frac{m_{OLP}}{m_{feed}} \times 100\% \qquad (3)$$

$$\text{Yield of coke } (\%) = \frac{m_{coke}}{m_{feed}} \times 100\% \qquad (4)$$

$$\text{Yield of gas } (\%) = 100 - \left(\frac{m_{OLP}+m_{coke}}{m_{feed}}\right) \times 100\% \qquad (5)$$

$$\text{Selectivity of gasoline } (\%) = \frac{m_{gasoline}}{m_{OLP}} \times 100\% \qquad (6)$$

$$\text{Selectivity of kerosene } (\%) = \frac{m_{kerosene}}{m_{OLP}} \times 100\% \qquad (7)$$

$$\text{Selectivity of diesel } (\%) = \frac{m_{diesel}}{m_{OLP}} \times 100\% \qquad (8)$$

3. Results and Discussion

3.1 Metal Composition of Catalysts by X-ray fluorescence (XRF) Analysis

To evaluate how base treatment affects the metal composition and Si/Al weight ratio of the Bayah's Natural Zeolite (BNZ) catalysts, X-ray fluorescence (XRF) analysis was conducted (Table 3). Table 3 presents the XRF results for BNZ catalysts modified with sodium hydroxide under varying NaOH concentrations using an ultrasound-assisted method. The data indicate that the untreated BNZ (BNZ-NT) catalyst contains the highest levels of silicon and aluminum, confirming its classification as a natural zeolite. These elements are used to calculate the Si/Al weight ratio. As shown in Table 3, sodium hydroxide treatment alters the Si/Al ratio, with treated samples exhibiting a lower ratio than the untreated catalyst. This reduction is attributed to the partial removal of silicon from the zeolite framework during desilication (Akyalcin *et al.*, 2019). A lower Si/Al ratio suggests that the alkaline treatment was effective, making the catalyst suitable for further testing in the hydrocracking process. Additionally, the treatment not only reduced the Si/Al ratio but also decreased the level of impurities (measured as metal content by weight). The most significant reduction in impurities was observed in the BNZ-3 sample. The XRF results also show that lower NaOH concentrations tend to reduce impurities more effectively, although the difference becomes less pronounced at higher concentrations. Excessively high NaOH levels result in only limited improvements in impurity removal.

3.2 Crystal Structure of Catalyst using X-ray Diffraction (XRD) Analysis

X-ray diffraction (XRD) analysis was carried out to examine the crystal structure of the catalysts. Specifically, the study aimed to assess how ultrasonic-assisted base treatment with varying NaOH concentrations (BNZ-1, BNZ-2, BNZ-3, and BNZ-4) affects the crystal structure of untreated BNZ (BNZ-NT). The diffraction patterns obtained were analyzed and compared with reference data from the Crystallography Open Database (COD) to identify the corresponding crystal phases. As illustrated in Figure 2, the XRD patterns of the NaOH-treated BNZ catalysts

Table 3.
Elemental metal composition of untreated- and treated-BNZ catalyst at various NaOH concentration.

Catalyst	Elemental metal content (wt%)				
	BNZ-NT	BNZ-1	BNZ-2	BNZ-3	BNZ-4
NaOH Concentration	-	(0.2 M)	(0.4 M)	(0.5 M)	(0.6 M)
Base Type for treatment	Non-treated	NaOH base solution treatment			
Si/Al weight ratio	5.388	4.833	4.659	4.681	4.651
Al	3.99	4.78	4.85	3.61	4.15
Si	21.5	23.1	22.6	16.9	19.3
Mg	0.247	0.221	0.197	0.218	0.172
P	0.019	-	-	-	-
K	2.15	1.19	1.07	0.809	0.924
Ca	1.52	0.124	0.182	0.138	0.163
Ti	0.102	0.083	0.094	0.041	0.066
Fe	0.759	0.508	0.521	0.349	0.426
Rb	0.008	0.004	0.005	0.005	0.004
Sr	0.044	0.006	0.009	0.007	0.009
Zr	0.017	0.012	0.012	0.012	0.014
Rh	0.095	-	-	-	-
Balance	69.6	69.9	70.4	77.9	74.7

display prominent peaks at 2θ values of 9.99°, 11.33°, 13.58°, 17.53°, 19.80°, 23.00°, 25.81°, 27.82°, 30.20°, and 32.90°. These peaks correspond to the crystal structures of Clinoptilolite-Ca, Mordenite and Heulandite-Ca, with COD reference codes 96-900-8266, 96-900-5608, and 96-900-0176, respectively. This confirms that the BNZ catalyst is a zeolite-based material composed of three distinct crystalline phases. Additionally, all samples exhibited a broad background peak in the 2θ range of 10°–33°, indicating some degree of amorphous content.

The X-ray Diffraction (XRD) analysis offers essential insight into the phase evolution of the synthesized materials, capturing the structural transition from the precursor (BNZ-NT) to the fully crystallized product (BNZ-4). The BNZ-4 sample exhibits sharp, well-defined diffraction peaks characteristic of a multi-phase crystalline system. The database matching using COD/JCPDS/ICDD references confirms the coexistence of three zeolitic phases: Clinoptilolite-Ca, Mordenite, and Heulandite-Ca. Quantitative Phase Analysis (QPA) identifies Clinoptilolite-Ca as the predominant phase (59.8%), with Mordenite (27.8%) and Heulandite-Ca (12.4%) present in smaller proportions. The abundance of distinct, high-intensity reflections across these phases clearly indicates that the final product is not a single-phase material but a composite zeolite system.

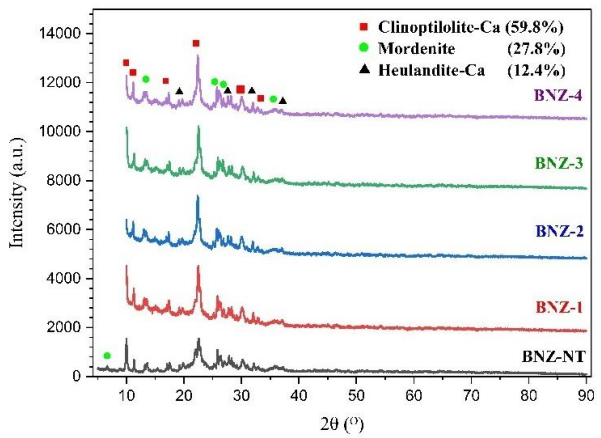

Fig. 2. XRD patterns of Bayah's Natural Zeolit (BNZ) catalysts modified by base treatment

3.3 Surface Area, Pore Diameter, Pore Volume, and Hierarchical Factor (HF) Characterizations by BET-BJH analysis

BET-BJH analysis was conducted to evaluate the particle characteristics of the catalysts, including surface area, pore diameter, pore volume, and the calculated Hierarchical Factor (HF). Table 4 presents the results of this characterization, detailing values for surface areas (S_{BET}, S_{meso}, S_{micro}, and S_{ext}), pore volumes (V_{total} and V_{micro}), average pore diameter, and the Hierarchical Factor (HF) for Bayah's Natural Zeolite catalysts treated with sodium hydroxide (NaOH) using an ultrasound-assisted method. In this study, the BNZ catalysts underwent desilication with varying NaOH concentrations, temperatures, and treatment durations. The results showed that surface area, pore volume, average pore diameter, and hierarchical factor improved following the base treatment in compared to untreated BNZ. Specifically, increasing NaOH concentration generally enhanced the particle properties of the catalysts. However, at 0.5 M NaOH, 65 °C, and 30 minutes, a decline in surface area was observed. Among the samples, BNZ-2 exhibited the highest surface area under the NaOH concentration variation. The greatest pore volume (V_{micro} and V_{total}) was recorded for BNZ-1, while BNZ-3 showed the most favorable results for average pore diameter and hierarchical

Table 4.
Particle properties (surface area, pore volume, pore diameter, and hierarchical factor) of Bayah's Natural Zeolite catalysts modified using NaOH solution with desilication method.

Catalyst	S_{BET}*	S_{meso}**	S_{micro}⁑	S_{ext}⁑	V_{micro}⁑	V_{total}⁂	Pore Diameter †	Hierarchical Factor (HF)‡
	($m^2.g^{-1}$)	($m^2.g^{-1}$)	($m^2.g^{-1}$)	($m^2.g^{-1}$)	($cm^3.g^{-1}$)	($cm^3.g_{-1}$)	nm	-
BNZ-NT	29.3	18.8	10.5	18.8	0.005	0.172	3.803	0.020
BNZ-1	229.3	39.0	190.3	39.0	0.098	0.341	3.830	0.049
BNZ-2	270.0	46.2	223.8	46.2	0.091	0.320	3.820	0.049
BNZ-3	222.7	42.0	180.7	42.0	0.093	0.255	3.838	0.069
BNZ-4	223.5	41.2	182.3	41.2	0.094	0.377	3.830	0.046
BNZ-5	226.2	38.8	187.4	38.8	0.096	0.369	3.831	0.045
BNZ-6	223.8	37.8	186.0	37.8	0.096	0.296	3.824	0.055
BNZ-7	214.2	44.3	169.9	44.3	0.088	0.283	3.818	0.064
BNZ-8	237.4	39.6	197.8	39.5	0.101	0.297	3.832	0.057

*Based on BET method; **S_{meso} is the result of subtracting S_{BET} with S_{micro}; ⁑Based on t-plot; ⁂Total pore volume at p/p° = 0.99; †Average pore diameter using BJH method based on N_2-desorption; ‡Hierarchical Factor (HF) is calculated using Equation (1).

factor, with values of 3.838 nm and 0.069, respectively. Significant improvement of surface area, pore diameter, pore volume, and considerable enhancement of Hierarchical Factor (HF) between untreated BNZ-NT and treated BNZ-x is caused by removal of entrapped impurities in the Bayah's natural zeolite and desilication effect due to the NaOH treatment. However, increasing pore diameter and pore volume leads to decreased surface area.

Variations in desilication temperature and duration led to an overall improvement in catalyst properties compared to the untreated catalysts. However, these enhancements were not as significant as those achieved through changes in NaOH concentration. For instance, the highest surface areas recorded for temperature and time variations were 226.2 m^2/g for BNZ-5 and 237.4 m^2/g for BNZ-8, respectively. In contrast, BNZ-2, which was influenced by NaOH concentration, exhibited the highest surface area overall at 270.0 m^2/g. Similarly, pore volume increased in line with surface area improvements. Among the catalysts, BNZ-5 and BNZ-8 showed the best performance for temperature and time variation, respectively. When considering average pore diameter and hierarchical factor, BNZ-3 stood out with the highest values, indicating it delivered the most optimal results under that condition.

According to the BET-BJH analysis results, BNZ-3 demonstrated the most favorable values for average pore diameter and hierarchical factor, while BNZ-2 exhibited the highest overall surface area. Figure 3 presents the nitrogen sorption isotherms, pore diameter size distributions, and hierarchical factors. The sorption isotherm illustrates the relationship between the amount of nitrogen adsorbed by the catalyst and the relative pressure (P/Po) at a constant temperature. As shown in Figure 3(a), the BNZ catalyst's nitrogen adsorption increases gradually at low P/Po values and continues to rise at higher P/Po. When P/Po nears 1, a sharp increase in adsorption was observ. This behavior is relatively modest due to the low Si/Al ratio (< 20), with BNZ catalyst values ranging from 4 to 5.4, resulting in only minor changes in porosity (Perez-Ramirez *et al*., 2008).

The adsorption behavior at low relative pressures (P/P_0 < 0.1) provides critical insight into the microporous characteristics of the treated zeolite samples. In this region, the isotherms exhibit a steep initial uptake, indicating the presence of abundant micropores formed during the desilication process. This observation is supported by the BET and t-plot analysis, which reveal significant micropore surface areas (S_{micro}) across all modified samples, with values exceeding 180 m^2/g for BNZ-2, BNZ-3, and BNZ-8. The corresponding micropore volumes (V_{micro}) range between 0.088 and 0.096 cm^3/g, confirming that the alkaline treatment effectively preserved and enhanced the intrinsic microporosity of the zeolite framework. The sharp adsorption at P/P_0 < 0.1, coupled with the high S_{micro} values, suggests that the hierarchical structure achieved through controlled desilication maintains strong microporous domains, which are essential for catalytic reactions requiring shape selectivity and diffusion within confined spaces. These findings demonstrate that, despite the introduction of mesoporosity at higher pressures, the microporous network remains dominant and structurally stable after NaOH treatment (Daou, J et al.,2022).

This indicates that both the treated and untreated BNZ catalysts exhibit a type IV adsorption isotherm, as classified by IUPAC. Type IV isotherms are characterized by adsorption behavior that mimics microporous materials at low relative pressures, while at higher pressures, a sharp increase in gas uptake occurs due to capillary condensation within mesopores (Fu *et al*., 2021). Therefore, it can be concluded that the BNZ catalyst possesses both microporous and mesoporous structures. This dual porosity contributes to the increase in surface area observed after base treatment. Additionally, the upward trend in the nitrogen adsorption isotherm curve confirms that the adsorption volume consistently rises across different treatment conditions, including variations in NaOH concentration, temperature, and desilication time.

The pore size distribution was evaluated using the BJH method, as illustrated in Figure 3(b). The results show that catalysts treated with a base solution through the desilication process exhibit an average pore diameter of around 3.8 nm. According to Dmitry Yu. Murzin (2020) finding, mesopores are defined as pores ranging from 2 nm to 50 nm in diameter. This indicates that both untreated and treated catalysts fall within the mesoporous range. Therefore, the change in average pore size due to base treatment does not represent a transition from micropores to mesopores, but rather a slight increase within the mesoporous range, indicating only a modest structural change (Murzin, 2020).

The pore size distribution (PSD) results indicate that the untreated sample (BNZ-NT) exhibits the highest intensity in the micropore region, with a sharp peak centered around 3–4 nm. After NaOH treatment, the intensity of this peak decreases slightly across all modified samples, suggesting partial removal or restructuring of micropores during desilication. However, the treated samples show a broader distribution extending into the

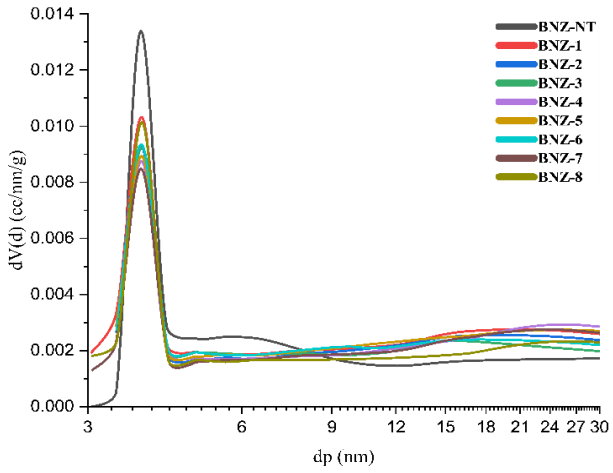

(a)

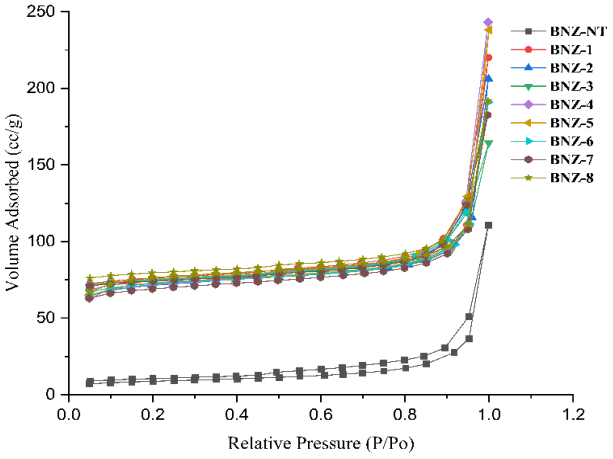

(b)

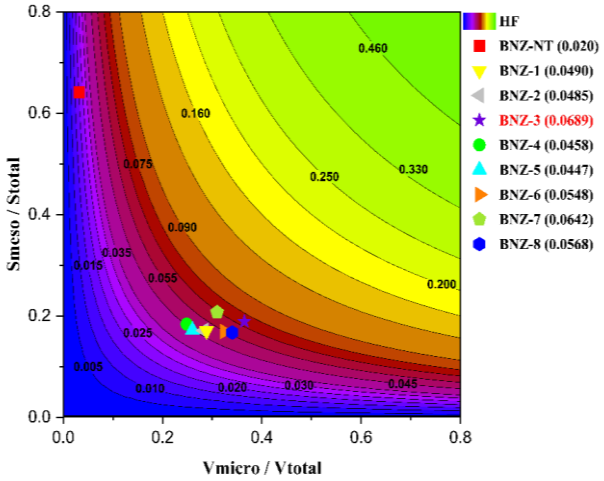

(c)

Fig. 3. N_2-sorption isotherm (a), pore diameter size distribution (b), and hierarchical factor (c), of base-treated and non-treated Bayah's Natural Zeolite catalyst.

mesopore range (10–30 nm), confirming the formation of secondary mesopores. This shift reflects the hierarchical nature of the modified zeolites, where mesoporosity is introduced without completely eliminating the original microporous framework. Such structural evolution is consistent with the mechanism of controlled desilication, which selectively extracts silicon to generate mesopores while preserving crystallinity. The presence of mesopores enhances molecular diffusion and accessibility to active sites, which is critical for catalytic applications involving bulky reactants. These findings align with recent studies emphasizing that alkaline treatment significantly increases mesopore volume and hierarchical factor while maintaining microporous domains essential for shape-selective catalysis (Wang *et al.*, 2025; Liu *et al.*, 2025; Shi *et al.*, 2021).

The Hierarchical Factor (HF), calculated using Equation (1), is illustrated in Figure 3(c). Introducing mesoporosity into hierarchical zeolites typically results in a reduction in micropore volume. This trend led to the development of a general metric known as the hierarchical factor (HF). It is represented as a contour plot based on the product of two ratios: the mesopore surface area to total surface area (S_{meso}/S_{total}) and the micropore volume to total pore volume (V^{micro}/V_{total}). This factor serves as a useful tool for classifying the porous structure of materials. An increase in the hierarchical factor is generally associated with enhanced catalytic performance (Chen *et al.*, 2020; Verboekend *et al.*, 2011).

As shown in Figure 3(c), the hierarchical factor (HF) increased following alkaline treatment with a sodium hydroxide (NaOH) solution. This increase correlates positively with higher NaOH concentrations and desilication temperatures, while it tends to decline with longer desilication times beyond a certain point. Among all the tested variables, the BNZ-3 catalyst exhibited the highest hierarchical factor. Specifically, BNZ-3 achieved an HF value of 0.069, which is more than three times greater than that of the untreated BNZ-NT catalyst, which had an HF value of 0.020.

Despite NaOH desilication introducing significant changes in the textural properties of zeolites, XRD patterns remain largely unchanged because the long-range crystalline framework is preserved. XRD primarily detects periodic atomic arrangements, which are not disrupted by partial silicon removal. In contrast, N_2 adsorption–desorption analysis reveals substantial increases in surface area and mesoporosity due to the formation of secondary pores during desilication. These local structural modifications enhance accessibility to active sites without compromising crystallinity, explaining the discrepancy between XRD and textural analysis results. Recent studies confirm that hierarchical zeolites produced via alkaline treatment exhibit stable mesopores and improved catalytic performance, while maintaining their original crystal phases (Roth *et al.*, 2025).

3.4 Base-treated BNZ Catalyst Performance Testing on Continuous Catalytic Hydrocracking of Palm Oil

The catalytic performance of Bayah's Natural Zeolite (BNZ) catalysts, modified with sodium hydroxide (NaOH), was assessed in a continuous fixed-bed reactor for the hydrocracking palm oil into biofuels such as gasoline, kerosene, and diesel. The primary output of this process is the organic liquid product (OLP), which serves as the crude form of biofuel, along with by-products including gas and coke. Figure 4 illustrates how different BNZ catalysts influence the distribution of hydrocracking products. As shown, OLP is the dominant product, accounting for approximately 80–86% of the total weight. Among the tested catalysts, BNZ-3, treated with ultrasound-assisted desilication using 0.5 M NaOH at 65 °C for 30 minutes, achieved the highest OLP yield at 85.67%. This suggests that an NaOH concentration of around 0.5 M, combined with moderate temperature and treatment duration, provides optimal conditions for maximizing biofuels yield.

At low NaOH concentrations, the increase in OLP (organic liquid product) yield is minimal compared to the untreated BNZ catalyst. Conversely, excessively high NaOH concentrations tend to reduce OLP yield while increasing the formation of by-products such as gas and coke, especially when compared to the performance of the BNZ-3 catalyst. Using ultrasonic-assisted stirring at lower temperatures results in a moderate OLP yield, whereas extending the desilication time under ultrasonic conditions leads to a decline in OLP production. As shown in Figure 4, the rise in OLP yield corresponds with increases in average pore diameter and the hierarchical factor, as detailed in Table 4. Larger pore diameter, greater pore volume, and higher hierarchical factor (HF) enhance the catalyst's ability to accommodate larger reactant molecules, such as triglycerides and intermediates, allowing them to access the internal surface of the catalyst more effectively. This demonstrates that improvements in these structural properties significantly boost liquid fuel production during the catalytic hydrocracking of palm oil.

Figure 5 illustrates the rise in HF value for the BNZ catalyst in relation to OLP yield. The HF value tripled compared to the untreated catalyst, leading to an increase in OLP production. However, when the concentration of NaOH used in the alkaline treatment becomes too high, its effect turns negative. Specifically, in the BNZ-4 variation (refer to Table 2), the yield drops again. This decline is attributed to excessive NaOH concentrations damaging the catalyst's pores, while very low concentrations have minimal impact. Among the variations, BNZ-3 shows the most optimal hierarchical factor (HF), as indicated in Figure 5.

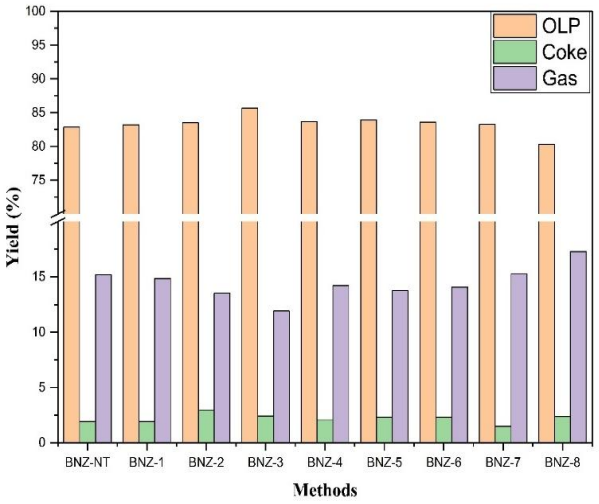

Fig. 4. Effect of the NaOH concentration, temperature, and time desilication on catalytic hydrocracking product distribution (See Table 2).

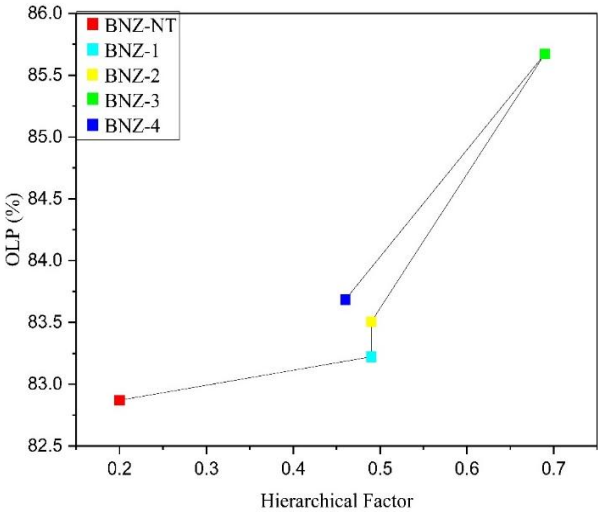

Fig. 5. Effect of hierarchical factor (HF) on the organic liquid product (OLP).

FT-IR (Fourier Transform Infrared) spectroscopy was used to analyze identification of the functional groups present in the resulting liquid products. The FT-IR spectra for both palm oil and the resulting liquid fuels are shown in Figure 6. The analysis reveals the presence of key functional groups in the biofuel, including esters, carboxylic acids, and hydrocarbons. The spectra also show a reduction in some peaks and the emergence of new ones, indicating chemical changes during the reaction. Both palm oil and the liquid products display absorption bands at 2922 cm^{-1} and 2853 cm^{-1}, which correspond to the asymmetric and symmetric stretching vibrations of C—H bonds in methylene groups (Coates *et al.*, 2000; Smith, 2018). These are further supported by a peak at 720 cm^{-1}, attributed to the rocking motion of C—H bonds in methylene groups (Smith, 2018). Additionally, a band at 1461 cm^{-1} is linked to the asymmetric and symmetric bending (umbrella mode) of C—H bonds in methyl groups. These features confirm the presence of hydrocarbon chains in both palm oil and the resulting fuels. In

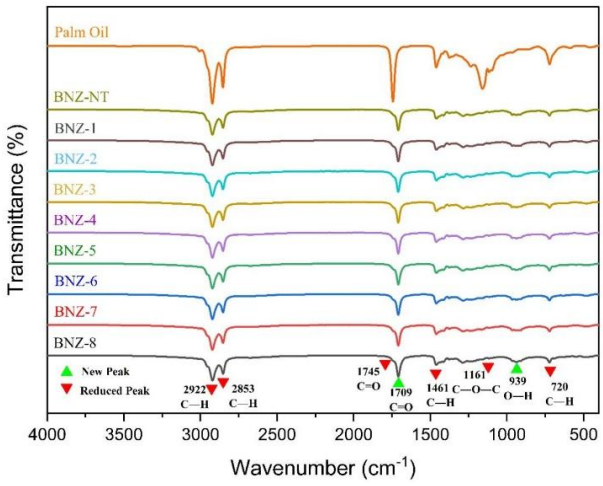

Fig. 6. FT-IR spectra of palm oil feed and organic liquid product at various catalysts.

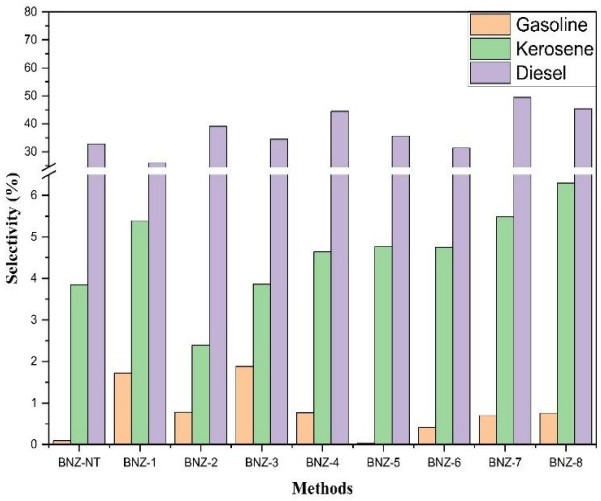

Fig. 7. Distribution of biofuels selectivity (i.e. gasoline, kerosene and diesel fractions) from the organic liquid product (OLP) based on the batch distillation.

palm oil specifically, the hydrocarbon chains are part of fatty acid structures, and a distinct absorption at 1745 cm^{-1} indicates the presence of a carbonyl (C=O) group, characteristic of ester bonds. The organic liquid products display new absorption bands at wavenumbers 1709 cm^{-1} and 939 cm^{-1}, which correspond to the stretching vibration of the carbonyl group (C=O) in carboxylic acids and the O−H vibration, respectively. The shift of the carbonyl absorption band from 1745 cm^{-1} in palm oil to 1709 cm^{-1} in the liquid products suggests a transformation of the carbonyl group from an ester to a carboxylic acid structure. Additionally, the reduction in the absorption band at 1161 cm^{-1}, associated with C−O−C vibrations, indicates the breakdown of the triglyceride structure, leading to the formation of carboxylic acids as intermediate compounds. The area under the 1745 cm^{-1} absorption peak can be used to quantify the conversion of ester bonds, which reflects the extent of triglyceride conversion.

The organic liquid product (OLP) is composed of gasoline, kerosene, and diesel fractions, which are separated based on their boiling point ranges through batch distillation at atmospheric pressure. Specifically, gasoline is collected between room temperature and 205 °C, kerosene between 205–310 °C, and diesel between 310–370 °C (Istadi *et al.*, 2023). Figure 7 shows how these biofuels components selectivity are distributed within the OLP, as determined by the distillation process. According to the figure, all BNZ catalysts that underwent desilication, using varying NaOH concentrations, temperatures, and durations of desilication, demonstrated a higher selectivity for the diesel fraction compared to kerosene and gasoline. However, the diesel fraction is not a reliable indicator of improved catalyst performance, as it still contains free fatty acids (FFAs), identified by carboxylic acid groups. One catalyst sample used in the hydrocracking process produced diesel with 1% carboxylic acid content (see Table 5). Therefore, the focus for enhancing biofuel selectivity is on increasing the yields of gasoline and kerosene (or aviation fuel) fractions. Among the tested catalysts, BNZ-3, treated with 0.5 M NaOH at 65 °C for 30 minutes, showed the most promising selectivity for the gasoline fraction.

Table 5.
Chemicals composition of organic liquid product (biofuels) of the catalytic hydrocracking palm oil over the promising BNZ-3 catalyst.

Composition	Weight Fraction (wt%)		
	Gasoline	Kerosene/avtuur	Diesel
Hydrocarbons	98.25	99.10	88.75
Alcohols	1.75	0	10.25
Esters	0	0.90	0
Carboxylic Acids	0	0	1.00

3.5 Chemical Composition of Biofuels Fraction

The chemical composition of the biofuel fractions (gasoline, kerosene, and diesel), obtained from the batch distillation process was analyzed using the GC-MS (Gas Chromatography-Mass Spectrometry) technique. According to the analysis, the main constituents of the organic liquid product derived from catalytic hydrocracking of palm oil fall into four categories: hydrocarbons, alcohols, esters, and acids, as detailed in Table 5. Hydrocarbons dominate all three fuel fractions, making up more than 88 wt%, with kerosene having the highest content (99.10 wt%), followed by gasoline (98.25 wt%) and diesel (88.75 wt%). In addition to hydrocarbons, the products also contain minor amounts of alcohols, esters, and acids. Notably, acids are absent in the gasoline and kerosene fractions, esters are not found in gasoline and diesel, and alcohols are missing from kerosene. The presence of a small amount of acid in the diesel fraction suggests that some triglycerides from palm oil first break down into free fatty acids, which are then converted into hydrocarbons through deoxygenation reactions such as decarboxylation (removal of CO_2), decarbonylation (removal of CO), and hydrodeoxygenation (removal of H_2O). Since hydrogen gas is used in the catalytic hydrocracking process, the primary reaction mechanisms involved include cracking, decarboxylation, decarbonylation, and hydrodeoxygenation.

Figure 8 presents a comparison of hydrocarbon distribution composition across the gasoline, kerosene, and diesel fractions. The gasoline fraction primarily contains hydrocarbons with carbon chains of C_8, C_9, and C_{11}, along with smaller amounts of C_{10}, C_{12}, and C_{15}. In the kerosene (or aviation fuel) fraction, the dominant hydrocarbons are C_{11}, C_{12}, and C_9, with minor contributions from C_8, C_{10}, C_{13}, C_{15}, C_{18}, C_{14}, and C_{20}. The diesel fraction mainly consists of C_{15}, C_{13}, C_{14}, C_{17}, and C_{18}, with smaller amounts of C_{11}, C_{12}, C_{16}, C_{19}, C_{24}, and C_{23}. These composition distributions suggest that the hydrocarbons in the gasoline and

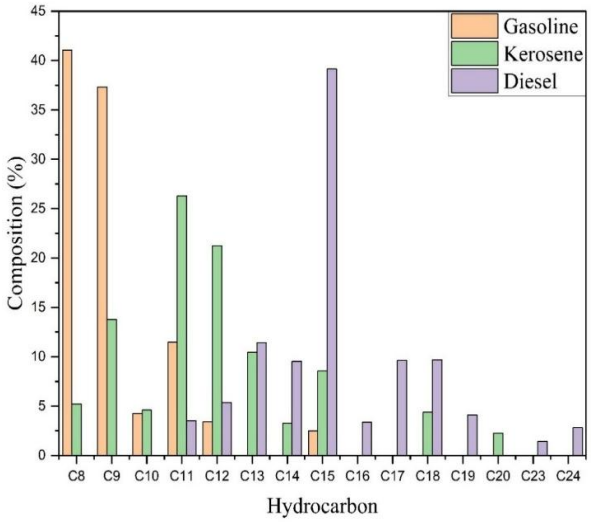

Fig. 8. Hydrocarbons distribution composition of gasoline, kerosene and diesel fractions.

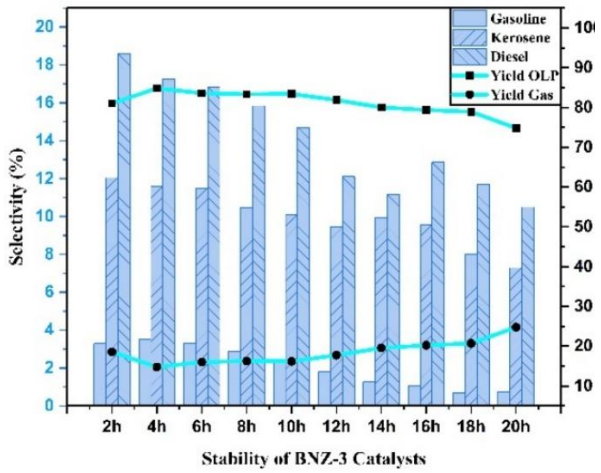

Fig. 9. Selectivity and yield performance of BNZ-3 catalyst during stability evaluation over extended reaction time

kerosene fractions are largely formed through cracking and hydrodeoxygenation reactions, while the diesel fraction is more likely produced via decarboxylation and decarbonylation processes.

3.6 Catalyst Stability and Coke Deposition on Catalyst

The stability of the natural Bayah-based catalysts was evaluated to determine their resistance to deactivation arising from coke deposition during hydrocracking. Coke formation is a persistent challenge in catalytic systems, as excessive carbonaceous buildup can restrict pore accessibility and consequently reduce catalytic activity. In this study, the most promising material, BNZ-3, was selected after undergoing a desilication treatment designed to enhance its textural characteristics. This modification was intended to increase porosity and thereby improve hydrocracking performance while mitigating the tendency for coke accumulation (Istadi et al., 2025).

The BNZ-3 catalyst was evaluated through a continuous stability test conducted under atmospheric pressure and hydrocracking conditions for up to 22 hours. Throughout the run, the product yield distribution and selectivity toward key biofuel fractions, gasoline, kerosene, and diesel, were systematically monitored. Such a pressure buildup is a well-known indicator of catalyst deactivation, as carbonaceous deposits can obstruct active sites, restrict pore accessibility, and elevate flow resistance within the reactor. The stability of the BNZ-3 catalyst was assessed by monitoring product selectivity and yield over a reaction period up to 22 hours. The bar chart (Figure 10) depicts the selectivity toward gasoline, kerosene, and diesel, while the accompanying line plots show the yields of organic liquid products (OLP) and gas. At the beginning of the reaction, gasoline selectivity was the highest, reaching approximately 18%, but it gradually declined with increasing time, indicating the onset of mild catalyst deactivation. In contrast, kerosene and diesel selectivity remained relatively steady with only minor variations, suggesting that BNZ-3 retains

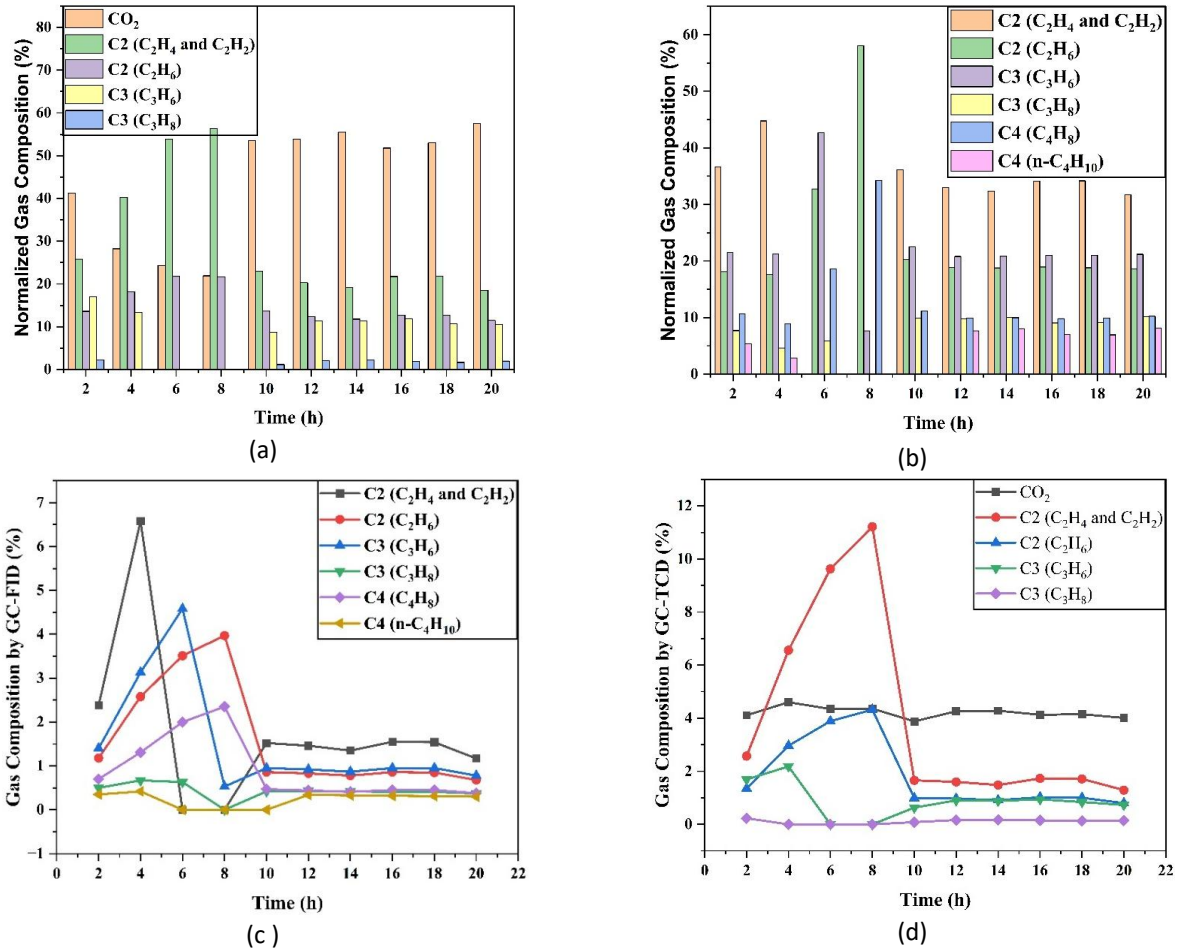

Fig. 10. a) Normalized gas composition over time on stream by GC-TCD analysis, b) Normalized gas composition over time on stream by GC-FID analysis, c) Gas composition by GC-FID analysis over time on stream, and d) Gas composition by GC-TCD analysis over time on stream.

moderate activity for producing middle-distillate fractions even during prolonged operation.

In terms of yield, the BNZ-3 catalyst exhibited stable performance throughout the duration of the test. The OLP yield consistently remained above 80%, with only a slight decline observed after 12 hours, while the gas yield stayed below 10%, indicating limited secondary cracking into gaseous products. This behavior demonstrates that BNZ-3 maintains strong hydrocracking stability and continues to favor liquid-phase product formation over extended reaction times. Overall, the results highlight BNZ-3 as a robust catalyst—showing high gasoline selectivity in the initial stages and sustained efficiency for kerosene and diesel production, making it well-suited for long-term hydrocracking applications.

Figure 10(a) shows the normalized GC-TCD profile, which represents the relative contributions of detected gases at each time point after scaling the raw signals to percentages rather than absolute amounts. In this view, C_2 species (primarily ethylene and ethane) dominate throughout most of the experiment, while CO_2 and C_3 exhibit intermittent increases. Normalization emphasizes compositional shifts rather than absolute production changes; for instance, a rise in C_2 percentage may result from either an increase in C_2 or a decrease in other species. Overall, the GC-TCD normalized data suggest a system oscillating between hydrocarbon-rich and more oxidized states, with C_2 consistently holding the largest fraction and CO_2 and C_3 contributing at specific intervals. This perspective is valuable for understanding relative speciation trends and potential changes in reaction selectivity over time.

Similarly, Figure 10(b) presents normalized GC-FID data, which primarily captures hydrocarbons due to the detector's sensitivity. C_2 hydrocarbons again dominate, while C_3 (propylene and propane) and C_4 (butylene and n-butane) show episodic increases, particularly in the mid-experiment phase. When C_3 and C_4 rise, the normalized share of C_2 declines, indicating temporary broadening of the product distribution toward heavier light ends. Because the data are normalized, these trends reflect selectivity dynamics rather than absolute yields. This behavior suggests that the process or catalyst undergoes phases favoring chain growth (C_2 to C_3/C_4), followed by a return to C_2 predominance, likely influenced by changes in surface coverage, active-site distribution, or operating conditions.

Figure 10(c) provides the actual GC-FID traces before normalization, revealing absolute hydrocarbon evolution and distinguishing true production events from compositional redistribution. A pronounced early transient is observed, with C_2 showing a sharp spike around 4–6 h, followed by a rapid decline to a near-steady regime. C_3 and C_4 exhibit smaller, localized maxima before stabilizing at low levels beyond 8 h. This profile indicates a start-up or activation phase characterized by high hydrocarbon formation rates, especially C_2, which later relax to steady-state values. Importantly, these actual data confirm that normalized trends in Figure 10(b) reflect genuine shifts in hydrocarbon formation rather than artifacts of scaling.

Finally, Figure 10(d) shows actual GC-TCD data for CO_2 and light hydrocarbons. CO_2 rises progressively to a mid-experiment maximum before stabilizing, while C2 and C3 display early transients and then converge to low, stable concentrations. This pattern suggests a temporal shift from hydrocarbon formation toward oxidation, with CO_2 becoming increasingly dominant as

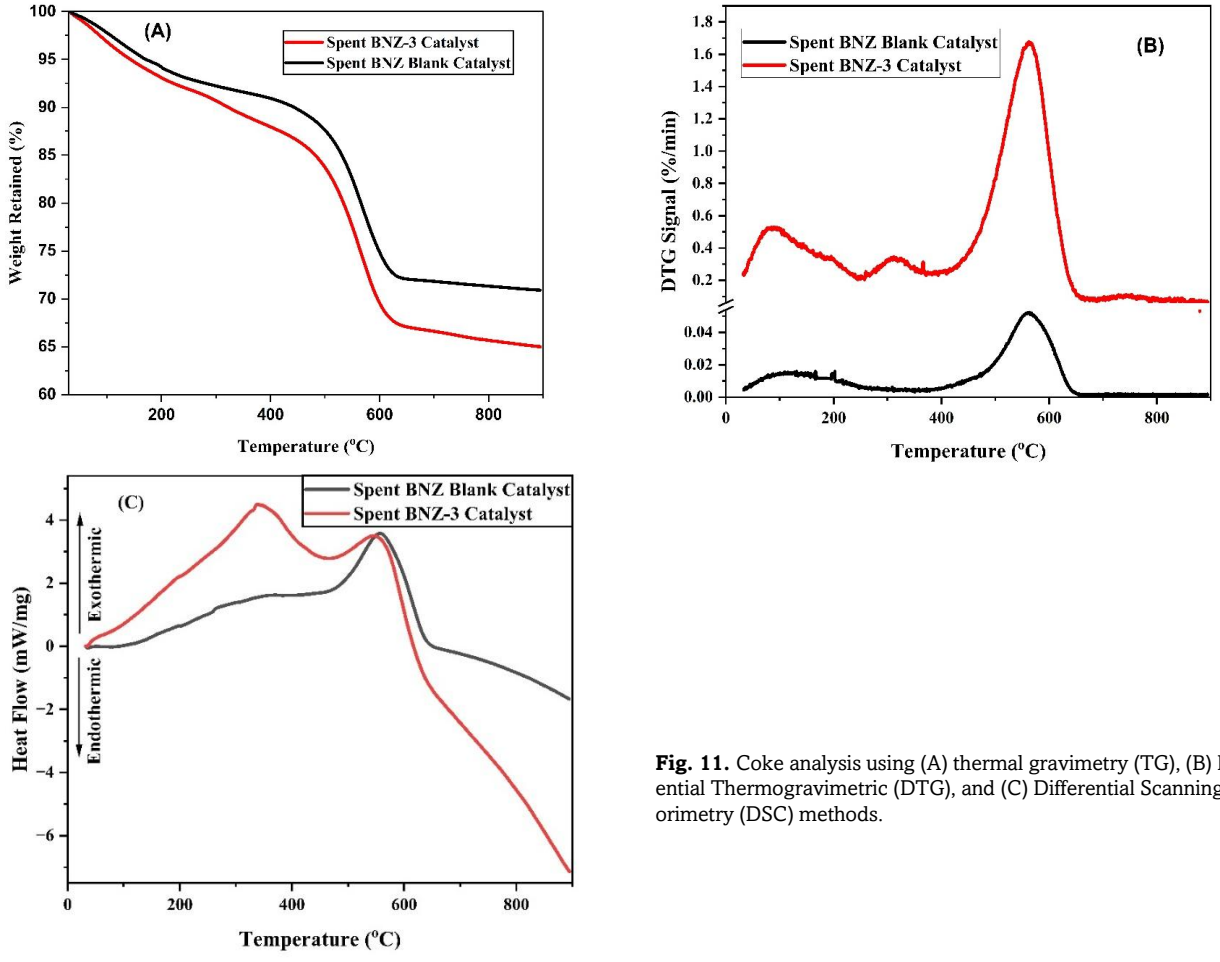

Fig. 11. Coke analysis using (A) thermal gravimetry (TG), (B) Differential Thermogravimetric (DTG), and (C) Differential Scanning Calorimetry (DSC) methods.

the run proceeds. Combined with the normalized view in Figure 10(a), these results indicate that even when hydrocarbons maintain a significant fractional presence, absolute CO_2 production can prevail during certain intervals. Thus, the actual GC-TCD data complement normalized profiles by clarifying when oxidation pathways intensify and when the system reaches steady-state in total gas output.

Figure 11(A) presents the thermogravimetric profiles of the spent BNZ-3 catalyst (red curve) and the spent BNZ blank catalyst (black curve) over a temperature range from ambient to approximately 900 °C. Both samples show an initial gradual weight loss below 200 °C, corresponding to the removal of physically adsorbed water and volatile species. This stage indicates the presence of minor moisture or light hydrocarbons prior to heating, with weight retention above 95%, confirming that the structural framework remains intact at low temperatures. As the temperature increases beyond 400 °C, a more pronounced weight loss is observed—particularly for BNZ-3, which exhibits a sharper decline than the blank catalyst. This behavior suggests that BNZ-3 accumulated a greater amount of carbonaceous deposits during the reaction, which decompose at elevated temperatures. Above 700 °C, both curves reach a plateau, indicating that most volatile and decomposable species have been removed, leaving behind the stable inorganic framework. Figure 11(b) shows the DTG curves, which illustrate the rate of weight loss as a function of temperature. The BNZ-3 catalyst displays two distinct decomposition peaks: a broad peak between 200–400 °C associated with the removal of adsorbed small amount of light hydrocarbons or organic residues, and a more pronounced peak near 600 °C corresponding to the rapid oxidation and decomposition of carbonaceous deposits or heavier hydrocarbons. The presence of multiple peaks indicates that BNZ-3 undergoes several degradation steps, reflecting a heterogeneous distribution of deposits with different thermal stabilities. The sharp and intense nature of these peaks further suggests substantial coke oxidation during heating. In contrast, the BNZ blank catalyst exhibits a much weaker DTG response across the entire temperature range, with only a small peak near 600 °C. This behavior indicates that the blank catalyst accumulated significantly less coke and possesses a more uniform surface composition, confirming its superior resistance to carbon deposition compared to BNZ-3.

Figure 11(c) presents the DSC profiles of both catalysts, offering insight into the heat flow associated with their thermal transformations. The BNZ-3 catalyst exhibits a pronounced exothermic peak between 400 °C and 700 °C, aligning with the major DTG peak observed in Figure 11(b). This exothermic response is characteristic of the oxidative decomposition of carbonaceous deposits, which release heat as they combust on the catalyst surface. The intensity of this peak indicates a substantial amount of coke oxidation, consistent with the greater weight loss recorded in the TG curve. In contrast, the BNZ blank catalyst shows only a modest exothermic peak within the same temperature range, confirming its lower accumulation of carbonaceous species. Overall, the DSC results corroborate the TG and DTG analyses, reinforcing the conclusion that BNZ-3 experiences more extensive coke deposition and undergoes more intense thermal decomposition than the blank catalyst. The blank catalyst's lower weight loss, weaker DTG signals, and minimal exothermic transitions highlight its superior thermal stability and suitability for applications requiring prolonged exposure to harsh thermal conditions. Conversely, while BNZ-3 demonstrates strong catalytic activity, its higher susceptibility to coke formation suggests that periodic regeneration may be necessary to sustain long-term performance.

4. Conclusion

The Bayah's Natural Zeolite (BNZ) catalysts were modified using an ultrasound-assisted sodium hydroxide (NaOH) treatment for desilication process of zeolite, with variations in NaOH concentration, treatment temperature, and duration. This treatment altered the physical and chemical properties of the catalysts. Characterization results revealed a reduction in the Si/Al weight ratio in the treated BNZ samples compared to the untreated version. The ultrasound-assisted NaOH treatment led to increased average pore diameter, pore volume, surface area, and the hierarchical factor (HF) of the catalysts. The crystal structure of the BNZ catalysts (BNZ-NT, BNZ-1 through BNZ-4) are Clinoptilolite-Ca, Mordenite and Heulandite-Ca. BNZ-5 to BNZ-8, were found to have similar crystalline structures. Among them, the BNZ-3 showed the most significant improvements, with an average pore diameter of 3.83 nm and a hierarchical factor (HF) of 0.069. These enhancements, larger pores, higher pore volume, considerable expanded surface area, and improved hierarchical factor (HF), enable better access for larger molecules like triglycerides and intermediates, improving the catalyst's effectiveness. As a result, these structural improvements significantly enhance liquid fuel production during the catalytic hydrocracking of palm oil. BNZ-3 emerged as the most promising catalyst, achieving an organic liquid product (OLP) yield of 85.67%, reaction conversion of 97.22% with hydrocarbon contents of 98.25 wt% in the gasoline fraction and 99.10 wt% in the kerosene/aviation fuel fraction. GC-MS analysis revealed that the primary constituents of gasoline, kerosene, and diesel were hydrocarbons, along with smaller amounts of compounds such as alcohols, esters, and acids. The DSC results corroborate the TG and DTG analyses, reinforcing the conclusion that BNZ-3 experiences more extensive coke deposition and undergoes more intense thermal decomposition than the blank catalyst. The blank catalyst's lower weight loss, weaker DTG signals, and minimal exothermic transitions highlight its superior thermal stability and suitability for applications requiring prolonged exposure to harsh thermal conditions.

Acknowledgments

The authors would like to express their sincere gratitude to Research Institution and Community Service, Universitas Diponegoro, Indonesia, for the financial support through the World Class Research Universitas Diponegoro (WCRU) research project category A with contract number: 118–22/UN7.6.1/PP/2021 (year 2021 – 2023).

Author Contributions: I. Istadi: Writing – review & editing, Writing – original draft, Supervision, Resources, Methodology, Formal analysis, Conceptualization, Validation Data curation. Wais Alqurni: Writing – original draft, Visualization, Methodology, Investigation, Formal analysis, Data curation. Teguh Riyanto: Writing – review & editing, Writing – original draft, Resources, Project administration, Methodology, Formal analysis.

Funding: This research was funded by Research Institution and Community Service, Universitas Diponegoro, Indonesia through the research project of World Class Research Universitas Diponegoro (WCRU) category A with contract number: 118–22/UN7.6.1/PP/2021.

Declaration of competing interest: The authors declare that they have no known competing financial interests or personal relationships that could have appeared to influence the work reported in this paper.

Data availability: Data will be made available on request.

Conflicts of Interest: The authors declare no conflict of interest.

References

Abelló, S., Bonilla, A., & Pérez-Ramírez, J. (2009). Mesoporous ZSM-5 zeolite catalysts prepared by desilication with organic hydroxides and comparison with NaOH leaching. *Applied Catalysis A: General*, 364(1–2), 191–198. https://doi.org/10.1016/j.apcata.2009.05.055 .

Akgül, M., & Karabakan, A. (2011). Promoted dye adsorption performance over desilicated natural zeolite. *Microporous and Mesoporous Materials,* 145(1–3), 157–164. https://doi.org/10.1016/j.micromeso.2011.05.012 .

Akyalcin, S., Akyalcin, L., & Bjørgen, M. (2019). Optimization of desilication parameters of low-silica ZSM-12 by Taguchi method. *Microporous and Mesoporous Materials*, 273, 256–264. https://doi.org/10.1016/j.micromeso.2018.07.014 .

Alaba, P. A., Sani, Y. M., Mohammed, I. Y., & Wan Daud, W. M. A. (2016). Insight into catalyst deactivation mechanism and suppression techniques in thermocatalytic deoxygenation of bio-oil over zeolites. *Reviews in Chemical Engineering*, 32(1). https://doi.org/10.1515/revce-2015-0025 .

Azhari, N. J., Mardiana, S., & Kadja, G. T. M. (2023). ZSM-48 zeolites with controllable mesopore formation: Synthesis, characterization, and catalytic performance. *Chemical Engineering Journal Advances,* 16, 100533. https://doi.org/10.1016/j.ceja.2023.100533 .

Aziz, I., Retnaningsih, T., Gustama, D., Saridewi, N., Adhani, L., & Dwiatmoko, A. A. (2021). Catalytic cracking of jatropha oil into biofuel over hierarchical zeolite supported NiMo catalyst. *AIP Conf. Proc.* 2349, 020004. https://doi.org/10.1063/5.0051737.

Aziz, I., Sugita, P., Darmawan, N., & Dwiatmoko, A. A. (2023). Effect of desilication process on natural zeolite as Ni catalyst support on hydrodeoxygenation of palm fatty acid distillate (PFAD) into green diesel. *South African Journal of Chemical Engineering*, 45, 328–338. https://doi.org/10.1016/j.sajce.2023.07.002 .

Aziz, I., Sugita, P., Darmawan, N., Dwiatmoko, A. A., & Rustyawan, W. (2024). Hydrodeoxygenation of palm fatty acid distillate (PFAD) over natural zeolite-supported nickel phosphide catalyst: Insight into Ni/P effect. *Case Studies in Chemical and Environmental Engineering,* 9, 100571. https://doi.org/10.1016/j.cscee.2023.100571.

Badan pusat statistik (BPS), (2025). Statistical Yearbook of Indonesia 2025. V 53, 2025. https://www.bps.go.id/id/publication.

Chen, L.-H., Sun, M.-H., Wang, Z., Yang, W., Xie, Z., & Su, B.-L. (2020). Hierarchically Structured Zeolites: *From Design to Application*. *Chemical Reviews,* 120(20), 11194–11294. https://doi.org/10.1021/acs.chemrev.0c00016 .

Coates, J. (2000). Interpretation of Infrared Spectra, A Practical Approach. In R. A. Meyers (Ed.), Encyclopedia of Analytical Chemistry (1st ed.). Wiley. https://doi.org/10.1002/9780470027318.a5606 .

Desmurs, L., Galarneau, A., Cammarano, C., Hulea, V., C. Vaulot, H. Nouali, B. Lebeau, T. J. Daou, C. Vieira Soares, G. Maurin, M. Haranczyk, I. Batonneau-Gener, A. Sachse, (2022) Determination of Microporous and Mesoporous Surface Areas and Volumes of Mesoporous Zeolites by Corrected *t*-Plot Analysis. *ChemNanoMat* 8, e202200051. https://doi.org/10.1002/cnma.202200051.

Dewanti, A. T., Rasyid, R., & Kalla, R. (2022). Effect of HCl/γ-Al2O3 and HCl/Ni/γ-Al2O3 Catalyst on The Cracking of Palm Oil. *Jurnal Kimia Valensi,* 8(2), 190–198. https://doi.org/10.15408/jkv.v8i2.25774 .

Fu, S., Fang, Q., Li, A., Li, Z., Han, J., Dang, X., & Han, W. (2021). Accurate characterization of full pore size distribution of tight sandstones by low-temperature nitrogen gas adsorption and high-pressure mercury intrusion combination method. *Energy Science & Engineering*, 9(1), 80–100. https://doi.org/10.1002/ese3.817 .

García, J. R., Bertero, M., Falco, M., & Sedran, U. (2015). Catalytic cracking of bio-oils improved by the formation of mesopores by means of Y zeolite desilication. *Applied Catalysis A: General*, 503, 1–8. https://doi.org/10.1016/j.apcata.2014.11.005 .

Guo, X., Guo, X.-N., Zhang, R. Q., Di, Z., Kang, B., Wei, Y., & Jia, J. (2024). Rational design on hierarchically porous Cu/ZSM-5 zeolite catalyst by protectively alkali-etching strategy. *Catalysis Today, 433*, 114656. https://doi.org/10.1016/j.cattod.2024.114656

Groen, J. C., Abelló, S., Villaescusa, L. A., & Pérez-Ramírez, J. (2008). Mesoporous beta zeolite obtained by desilication. *Microporous and Mesoporous Materials,* 114(1–3), 93–102. https://doi.org/10.1016/j.micromeso.2007.12.025 .

Groen, J. C., Moulijn, J. A., & Pérez-Ramírez, J. (2006). Desilication: On the controlled generation of mesoporosity in MFI zeolites. *J. Mater. Chem.*, 16(22), 2121–2131. https://doi.org/10.1039/B517510K.

Groen, J. C., Peffer, L. A. A., Moulijn, J. A., & Pérez-Ramírez, J. (2005). Mechanism of Hierarchical Porosity Development in MFI Zeolites by Desilication: The Role of Aluminium as a Pore-Directing Agent. *Chemistry – A European Journal*, 11(17), 4983–4994. https://doi.org/10.1002/chem.200500045 .

Groen, J., Sano, T., Moulijn, J., & Perezramirez, J. (2007). Alkaline-mediated mesoporous mordenite zeolites for acid-catalyzed conversions☆. *Journal of Catalysis*, 251(1), 21–27. https://doi.org/10.1016/j.jcat.2007.07.020 .

Istadi, I., Kusumawati, Y., Riyanto, T., Anggoro, D. D., Jongsomjit, B., & Putranto, A. B. (2024). Enhancing spent RFCC catalysts for biofuel production: Ultrasound-assisted acid treatment for improved crystallinity, pore size, and acid site ratio. *Case Studies in Chemical and Environmental Engineering*, *10*, 100843. https://doi.org/10.1016/j.cscee.2024.100843

Istadi, I., Riyanto, T., Anggoro, D. D., Pramana, C. S., & Ramadhani, A. R. (2023). High Acidity and Low Carbon-Coke Formation Affinity of Co-Ni/ZSM-5 Catalyst for Renewable Liquid Fuels Production through Simultaneous Cracking-Deoxygenation of Palm Oil. *Bulletin of Chemical Reaction Engineering & Catalysis*, 18(2), 222–237. https://doi.org/10.9767/bcrec.17974 .

Istadi, I., Riyanto, T., Buchori, L., Anggoro, D. D., Gilbert, G., Meiranti, K. A., & Khofiyanida, E. (2020). Enhancing Brønsted and Lewis Acid Sites of the Utilized Spent RFCC Catalyst Waste for the Continuous Cracking Process of Palm Oil to Biofuels. *Industrial & Engineering Chemistry Research,* 59(20), 9459–9468. https://doi.org/10.1021/acs.iecr.0c01061 .

Istadi, I., Riyanto, T., Khofiyanida, E., Buchori, L., Anggoro, D. D., Sumantri, I., Putro, B. H. S., & Firnanda, A. S. (2021). Low-oxygenated biofuels production from palm oil through hydrocracking process using the enhanced Spent RFCC catalysts. *Bioresource Technology Reports*, 14, 100677. https://doi.org/10.1016/j.biteb.2021.100677 .

Istadi, I., Riyanto, T., Salsabilla, A., & Qotrunnada, N. A. (2025). Comparative study on the characteristics and performance of Ni-impregnated and non-impregnated natural zeolite catalysts in the hydrocracking of palm oil to biofuels. *Journal of Chemical Engineering Research Progress,* 2(2), 254–262. https://doi.org/10.9767/jcerp.20527

Kadarwati, S., & Wahyuni, S. (2015). Characterization and Performance Test of Palm Oil Based Bio-Fuel Produced Via Ni/Zeolite-Catalyzed Cracking Process. *International Journal of Renewable Energy Development,* 4(1), 32–38. https://doi.org/10.14710/ijred.4.1.32-38.

Karim, T. M., Toyoda, H., Sawada, M., Zhao, L., Wang, Y., Xiao, P., Wang, L., Huang, J., & Yokoi, T. (2024). Aluminum distribution on the microporous and hierarchical ZSM-5 zeolite catalysts and its effect on catalytic performance. *Chem & Bio Engineering*, 1(9), 805–816. https://doi.org/10.1021/cbe.4c00117

Li, T., Krumeich, F., Chen, M., Ma, Z., & Van Bokhoven, J. A. (2020). Defining aluminum-zoning during synthesis of ZSM-5 zeolites. *Physical Chemistry Chemical Physics*, 22(2), 734–739. https://doi.org/10.1039/C9CP05423E .

Liu, H., Liu, G., Zhang, Z., Si, N., Wang, X., Chang, P., & Barakos, G. (2025). Improved characterization of the pore size distribution in full and across scale by a fractal strategy. *Physics of Fluids, 37*(4), 046602. https://doi.org/10.1063/5.0260442

Long, F., Zhai, Q., Liu, P., Cao, X., Jiang, X., Wang, F., Wei, L., Liu, C., Jiang, J., & Xu, J. (2020). Catalytic conversion of triglycerides by metal-based catalysts and subsequent modification of molecular

structure by ZSM-5 and Raney Ni for the production of high-value biofuel. *Renewable Energy*, 157, 1072–1080. https://doi.org/10.1016/j.renene.2020.05.117 .

Mamman, J. T., Toyoda, H., Sawada, M., Zhao, L., Wang, Y., Xiao, P., Wang, L., Huang, J., & Yokoi, T. (2022). Aluminum distribution on the microporous and hierarchical ZSM-5 zeolite catalysts and its effect on catalytic performance. *Journal of Porous Materials*, 29(5), 1349–1362. https://doi.org/10.1007/s10934-022-01239-9

Mokrzycki, Ł., Sulikowski, B., & Olejniczak, Z. (2009). Properties of Desilicated ZSM-5, ZSM-12, MCM-22 and ZSM-12/MCM-41 Derivatives in Isomerization of α-Pinene. *Catalysis Letters*, 127(3–4), 296–303. https://doi.org/10.1007/s10562-008-9678-z .

Mortensen, P. M., Grunwaldt, J.-D., Jensen, P. A., Knudsen, K. G., & Jensen, A. D. (2011). A review of catalytic upgrading of bio-oil to engine fuels. *Applied Catalysis A: General*, 407(1–2), 1–19. https://doi.org/10.1016/j.apcata.2011.08.046.

Murzin, D. (2020). Engineering catalysis (2nd edition). De Gruyter. https://doi.org/10.1515/9783110614435 .

Nasikin, M., Susanto, B.H., Hirsaman, M.A., dan Wijanarko, A., (2009), Bio-gasoline from Palm Oil by Simultaneous Cracking and Hydrogenation Reaction over NiMo/zeolite Catalyst, *World Applied Sciences Journal*, 5 (Special Issue for Environment), 74-79.

Oliveira, D. S., Lima, R. B., Pergher, S. B. C., & Caldeira, V. P. S. (2023). Hierarchical Zeolite Synthesis by Alkaline Treatment: Advantages and Applications. *Catalysts,* 13(2), 316. https://doi.org/10.3390/catal13020316 .

Oruji, S., Khoshbin, R., & Karimzadeh, R. (2018). Preparation of hierarchical structure of Y zeolite with ultrasonic-assisted alkaline treatment method used in catalytic cracking of middle distillate cut: The effect of irradiation time. *Fuel Processing Technology*, 176, 283–295. https://doi.org/10.1016/j.fuproc.2018.03.035 .

Panarmasar, N., Hinchiranan, N., & Kuchonthara, P. (2022). Catalytic hydrotreating of palm oil for bio-jet fuel production over Ni supported on mesoporous zeolite. *Materials Today: Proceedings,* 57, 1082–1087. https://doi.org/10.1016/j.matpr.2021.09.385 .

Pérez-Ramírez, J., Christensen, C. H., Egeblad, K., Christensen, C. H., & Groen, J. C. (2008). Hierarchical zeolites: Enhanced utilisation of microporous crystals in catalysis by advances in materials design. *Chemical Society Reviews*, 37(11), 2530. https://doi.org/10.1039/b809030k .

Riyanto, T., Istadi, I., Jongsomjit, B., Anggoro, D. D., Pratama, A. A., & Faris, M. A. A. (2021). Improved Brønsted to Lewis (B/L) Ratio of Co- and Mo-Impregnated ZSM-5 Catalysts for Palm Oil Conversion to Hydrocarbon-Rich Biofuels. *Catalysts,* 11(11), 1286. https://doi.org/10.3390/catal11111286 .

Roth, W. J., Gil, B., Tarach, K. A., & Góra-Marek, K. (2025). Top-down engineering of zeolite porosity. *Chemical Society Reviews, 54*(13), 7484–7560. https://doi.org/10.1039/D5CS00319A

Seifi, H., & Sadrameli, S. M. (2016). Improvement of renewable transportation fuel properties bydeoxygenation process using thermal and catalytic cracking of triglycerides and their methyl esters. *Applied Thermal Engineering*, 100, 1102–1110. https://doi.org/10.1016/j.applthermaleng.2016.02.022 .

Shi, K., Santiso, E. E., & Gubbins, K. E. (2021). Current advances in characterization of nano-porous materials: Pore size distribution and surface area. In *Porous Materials* (pp. 315–340). Springer. https://doi.org/10.1007/978-3-030-65991-2_12

Smith, B. (2018). Infrared Spectral Interpretation: A Systematic Approach (1st ed.). CRC Press. https://doi.org/10.1201/9780203750841 .

Verboekend, D., & Pérez-Ramírez, J. (2011). Design of hierarchical zeolite catalysts by desilication. *Catalysis Science & Technology*, 1(6), 879. https://doi.org/10.1039/c1cy00150g .

Verboekend, D., Vilé, G., & Pérez-Ramírez, J. (2012). Mesopore Formation in USY and Beta Zeolites by Base Leaching: Selection Criteria and Optimization of Pore-Directing Agents. *Crystal Growth & Design*, 12(6), 3123–3132. https://doi.org/10.1021/cg3003228.

Wang, Z., Gao, L., Zhong, X., Zhang, Y., Shakeri, M., Zhang, X., & Zhang, B. (2025). Accurately tuning the pore size and acidity of mesoporous zeolites for enhancing the catalytic hydrocracking of polypropylene. *Journal of Materials Chemistry A, 13*(2875–2883). https://doi.org/10.1039/D4TA07329K

Yin, X., Li, Z., Wang, S., Chu, N., Yang, J., & Wang, J. (2015). Hydrothermal synthesis of hierarchical zeolite T aggregates using tetramethylammonium hydroxide as single template. *Microporous and Mesoporous Materials,* 201, 247–257. https://doi.org/10.1016/j.micromeso.2014.09.018 .

Zheng, Z., Wang, J., Wei, Y., Liu, X., Yu, F., & Ji, J. (2019). Effect of La-Fe/Si-MCM-41 catalysts and CaO additive on catalytic cracking of soybean oil for biofuel with low aromatics. *Journal of Analytical and Applied Pyrolysis,* 143, 104693. https://doi.org/10.1016/j.jaap.2019.104693 .

© 2026. The Author(s). This article is an open access article distributed under the terms and conditions of the Creative Commons Attribution-ShareAlike 4.0 (CC BY-SA) International License (http://creativecommons.org/licenses/by-sa/4.0/)